HIGH-FIDELITY MULTIPLE-FLYBY TRAJECTORY OPTIMIZATION USING MULTIPLE SHOOTING

Donald H. Ellison, [*]
Jacob A. Englander [†]

Rendering a complex spacecraft trajectory in high fidelity can be an expensive endeavor, both computationally and from a human time/cost standpoint. However, in many cases, a low-fidelity trajectory that reasonably approximates a high-fidelity counterpart is much easier to obtain. Thus, it is important to have an efficient process for converting a trajectory from lower-fidelity model to high fidelity. We present a method for converting low-fidelity trajectories into high fidelity that relies on multiple shooting, nonlinear programming, and numerical integration. The procedure converts any zero-radius sphere-of-influence gravity-assist events to fully integrated flyby events. Several numerical examples are presented that showcase the flexibility of the high-fidelity rendering process across multiple mission types and flight regimes.

INTRODUCTION

The design of a planetary science mission involves many challenges, one of which is that the trajectory design team will undoubtedly be asked to deliver trajectory solutions during any stage of the design process, and at correspondingly different levels of fidelity. For example, during the earliest stages of a mission design campaign, multiple solution families might be identified using low-fidelity techniques such as patched conics, or solving Lambert's problem in grid based. Later phases of a mission design will require higher fidelity trajectory renderings that are computed with more accurate dynamics models and include fully featured, non-instantaneous event modeling for activities such as launch vehicle injection, flybys and orbit insertions. A robust design workflow must not only feature tools and techniques for producing trajectory solutions at any fidelity level, but ideally it will also enforce process requirements that ensure that the transition of solutions from lower-fidelity models to flight fidelity is reproducible and achieved with minimal human-in-the-loop activity.

Traditionally, one of the most time-consuming aspects of continuing a solution from an initial low-fidelity broad search to a high-fidelity point design is the final high-fidelity rendering of the trajectory [a]. Previous studies have described the continuation of zero-radius sphere-of-influence (ZSOI) trajectories to high fidelity,[1] as well as the use of multiple-shooting techniques to render flight-fidelity trajectories.[2] These investigations focused on using differential correction to account for discrepancies between solutions in lower-fidelity regimes and those in higher-fidelity models. The current work seeks to achieve the same objective—being the development of a reliable method for transitioning low-fidelity trajectories to high fidelity—but does so using more robust nonlinear programming (NLP) techniques. While nonlinear programming brings with it increased implementation complexity, it also offers the capability of locally optimizing the final end-to-end high-fidelity solution.

This work describes an automated work flow for computing trajectories with fully modeled gravity assist events from an initial guess that uses ZSOI flybys. The dynamics and transcriptions used for both low- and high-fidelity modeling are described. A technique for generating a high-fidelity initial guess from the low-fidelity ZSOI trajectory is introduced, and its range of applicability is discussed. Subtleties related to the state representation of the spacecraft and numerical integration of the trajectory are also presented. The methods described in this paper have been implemented in the Evolutionary Mission Trajectory Generator (EMTG)[3–5] and the conversion of a ZSOI trajectory into

---

[1]Aerospace Engineer, NASA Goddard Space Flight Center, Navigation and Mission Design Branch, 8800 Greenbelt Rd, Greenbelt, MD 20771, Member AAS

[2]Aerospace Engineer, NASA Goddard Space Flight Center, Navigation and Mission Design Branch, 8800 Greenbelt Rd, Greenbelt, MD 20771, Member AAS

[a]In this work, a high-fidelity trajectory solution is considered one that is computed using explicit numerical integration and that models the following accelerations: central-body point-mass gravity and oblateness, third-body point-mass gravity sources and solar radiation pressure (SRP)

American Institute of Aeronautics and Astronautics

high fidelity using this procedure is demonstrated on two challenging planetary trajectory design problems: Lucy[6,7] and a notional gas giant capture scenario both solved using EMTG.

HIGH-FIDELITY MULTIPLE SHOOTING

The trajectory transcriptions described in this work are all based on direct two point shooting as illustrated in Figure 1. This optimization method involves propagating the spacecraft forward in time from the left phase boundary and backwards in time from the right phase boundary. The primary set of constraints imposed on the optimizer are the "match point" constraints $\mathbf{c}_{\mathrm{mp}}$:

$$
\mathbf{c}_{\mathrm{mp}} = \mathbf{X}_{\mathrm{mp}}^{\mathrm{B}} - \mathbf{X}_{\mathrm{mp}}^{\mathrm{F}} = \begin{bmatrix} \mathbf{r}^{\mathrm{B}} - \mathbf{r}^{\mathrm{F}} \\ \mathbf{v}^{\mathrm{B}} - \mathbf{v}^{\mathrm{F}} \\ m^{\mathrm{B}} - m^{\mathrm{F}} \end{bmatrix} = \mathbf{0},
\tag{1}
$$

where $\mathbf{X}$ is the spacecraft state vector, the F superscript indicates the left-hand side of the match point and the B superscript indicates the right-hand side of the match point.

The two-point shooting method supports a wide variety of trajectory models, however, this work focuses on the multiple gravity assist with n deep space maneuvers using shooting (MGAnDSMs) model.[4,8,9]
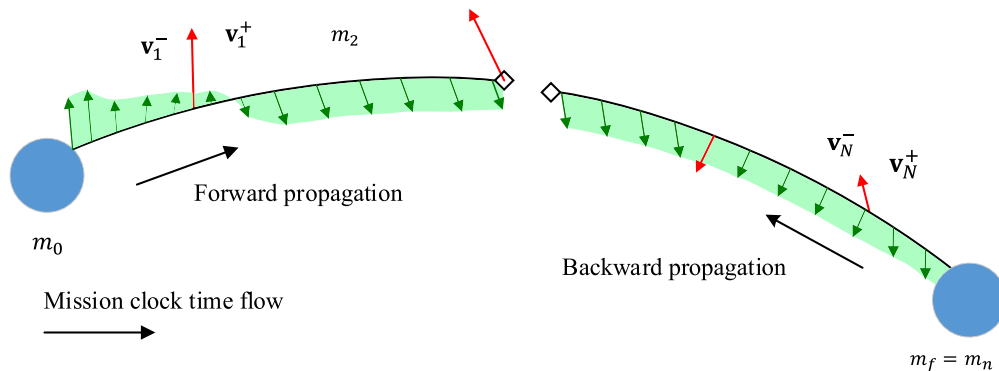

Figure 1: Two point high-fidelity shooting modeling of an n-maneuver chemical trajectory phase.

The MGAnDSMs transcription is a direct optimization method, in which the spacecraft trajectory is parameterized as an NLP that can be locally optimized using a solver such as the Sparse Nonlinear Optimizer (SNOPT)[10] or the Interior Point OPTimizer (IPOPT).[11] Recent research has shown that when a robust local NLP solver is paired with a stochastic search heuristic such as monotonic basin hopping (MBH),[5,12–14] the effectiveness of the combined local search method is greatly enhanced. This approach is used for solving the example trajectory design problems presented in this paper. A typical set of NLP decision variables for an MGAnDSMs phase are described in Table 1.

Table 1: Decision variables for an MGAnDSMs phase.

x_i	Description
t_{launch}	Launch epoch
v_∞	Launch impulse magnitude
RA	Right ascension of launch asymptote
DEC	Declination of launch asymptote
Δt_p	Phase time of flight
m_{f_p}	Phase final mass
$\mathbf{v}_{\infty_p}(t_0)$	Phase initial excess velocity vector
$\mathbf{v}_{\infty_p}(t_f)$	Phase final excess velocity vector
Δt_1	time to first maneuver
$\Delta t_2, ..., \Delta t_n$	inter-maneuver times
Δt_{n+1}	time from last maneuver to phase end
$\Delta \mathbf{v}_1, ..., \Delta \mathbf{v}_n$	DSM vectors

The MGAnDSMs model, in conjunction with the trajectory transcriptions described in the high-fidelity launch and flyby sections, can be used with low-fidelity dynamics models (e.g., two body Keplerian propagation). However, the example problems that will be discussed later in this paper are optimized with a high-fidelity acceleration model that incorporates gravitational forces from i perturbing bodies, SRP, and central body oblateness. These natural trajectory perturbations are represented by the green highlighted arrows in Figure 1. The MGAnDSMs model supports the inclusion of n chemical maneuvers during any trajectory phase (Figure 1 shows an example four-maneuver phase). The equations of motion that model the spacecraft motion and mass during a finite burn event are:

$$\ddot{\mathbf{r}} = -\frac{\mu_{\mathrm{cb}}}{r^2}\frac{\mathbf{r}}{r} - \sum_{j=1}^{i} \mu_j \left(\frac{\mathbf{r} - \mathbf{r_j}}{\|\mathbf{r} - \mathbf{r_j}\|^3} + \frac{\mathbf{r_j}}{r_j^3} \right) + \ddot{\mathbf{r}}_{\mathrm{SRP}} + \ddot{\mathbf{r}}_{J_2} + \frac{D\,T}{m}\mathbf{u} \tag{2}$$

$$\dot{m} = -\|\mathbf{u}\|\, D\, \dot{m}_{\max} \tag{3}$$

In Eq. (2) μ_{cb} is the gravitational parameter of the central body, μ_j is the gravitational parameter of the jth perturbing gravitational body, m is the mass of the spacecraft, $\mathbf{r}$ is the position vector of the spacecraft with respect to the central body, and $\mathbf{r_j}$ is the position vector of the jth body with respect to the central body, D is the duty cycle of the thruster, and T is the maximum thrust of the chemical rocket motor. The variable $\mathbf{u}$ is an up-to-unit vector that allows the optimizer to modulate the thrust level. If maneuvers are modeled as impulsive the equations of motion become:

$$\ddot{\mathbf{r}} = -\frac{\mu_{\mathrm{cb}}}{r^2}\frac{\mathbf{r}}{r} - \sum_{j=1}^{i} \mu_j \left(\frac{\mathbf{r} - \mathbf{r_j}}{\|\mathbf{r} - \mathbf{r_j}\|^3} + \frac{\mathbf{r_j}}{r_j^3} \right) + \ddot{\mathbf{r}}_{\mathrm{SRP}} + \ddot{\mathbf{r}}_{J_2} \tag{4}$$

$$\mathbf{v}_k^+ = \mathbf{v}_k^- + \Delta\mathbf{v}_k \tag{5}$$

$$\dot{m}_k^+ = m_k^- e^{-\Delta\mathbf{v}_k/v_e} \tag{6}$$

$$\tag{7}$$

where the $-/+$ superscripts indicate pre- and post-burn values respectively, the subscript $k \in \{1, ..., n\}$ refers to the kth maneuver in the phase and v_e is the exhaust velocity of the rocket motor.

TRAJECTORY BOUNDARY CONDITIONS

The EMTG software implementation is capable of including several different types of boundary events into a trajectory optimization problem. The boundary types that are the focus of this work are ephemeris-pegged boundary (EPB)s and ephemeris-referenced boundary (ERB) events.

Ephemeris-Pegged Boundary

The first class of boundary condition examined in this paper is the EPB condition. An EPB is a trajectory phase boundary that shares a position with an object located in the optimizer's ephemeris system (SPICE[15]). The ZSOI flyby model is an example of an EPB since the event is modeled as an instantaneous change in the spacecraft's velocity at the position of the target flyby body.

Ephemeris-Referenced Boundary

The second class of boundary condition considered in this work is the ERB. This class of boundary condition describes an event that occurs at a phase boundary whose position is displaced relative to an ephemeris position (i.e., the position is resolved via vector addition from an ephemeris position). Examples of ERBs are periapse boundaries and events on a body's sphere of influence (SOI). Two specific ERB examples will be discussed in this work: a high-fidelity departure from an Earth parking orbit and a high-fidelity gravity assist maneuver.

HIGH-FIDELITY FLYBY

A basic high-fidelity flyby event is comprised of three separate boundary events with trajectory "shooters" located at each boundary event: an encounter with the exterior of the flyby target's SOI, periapse passage of the flyby target, and an encounter with the interior of the flyby target's SOI. The multiple shooting problem that transcribes a flyby event is illustrated in Figure 2, with trajectory match point defect constraint vectors denoted by $\mathbf{c}_{\mathrm{mp}}$ and the boundary shooting locations identified with the small circles.

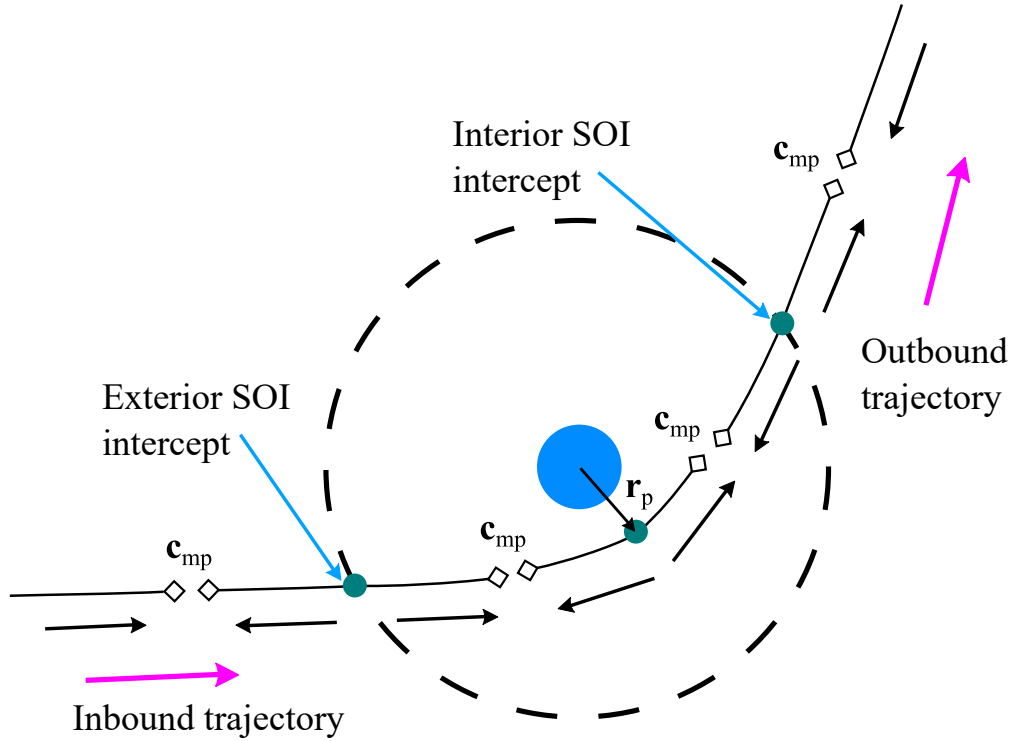American Institute of Aeronautics and Astronautics

Figure 2: Ephemeris-referenced gravity-assist multiple-shooting transcription.

At the three boundary-event locations, the spacecraft's state is encoded as optimizer decision variables using spherical coordinates in the flyby body-centered International Celestial Reference Frame (ICRF) (Table 2). Note that the magnitude of the spacecraft's position r is not an optimization decision variable as the SOI of the target flyby body is set *a priori* by the user.

Table 2: Ephemeris-referenced boundary event decision variables.

Parameter	Description
RA	spacecraft position vector right ascension
DEC	spacecraft position vector declination
v	spacecraft velocity vector magnitude
vRA	spacecraft velocity vector right ascension
$vDEC$	spacecraft velocity vector declination
m	spacecraft mass

For the exterior/interior SOI boundary events, the spacecraft position vector magnitude r is not encoded as a decision variable, as these events are assumed to occur on the flyby target's SOI, whose radius is predefined. Therefore, r is known *a priori*. The times of flight from SOI to periapse (Δt_in) and then from periapse back out to the SOI (Δt_out) are also optimizer decision variables. At the flyby periapse boundary location, the periapse condition is enforced by constraining the inner product of the position and velocity vectors to be zero:

$$\mathbf{r} \cdot \mathbf{v} = 0 \tag{8}$$

HIGH-FIDELITY LAUNCH

In order to model high-fidelity launch scenarios, the multiple-shooting transcription shown in Figure 2 is modified to enable departure from a parking orbit. In Figure 3, the green circle represents a boundary event located outside the departure body's SOI.

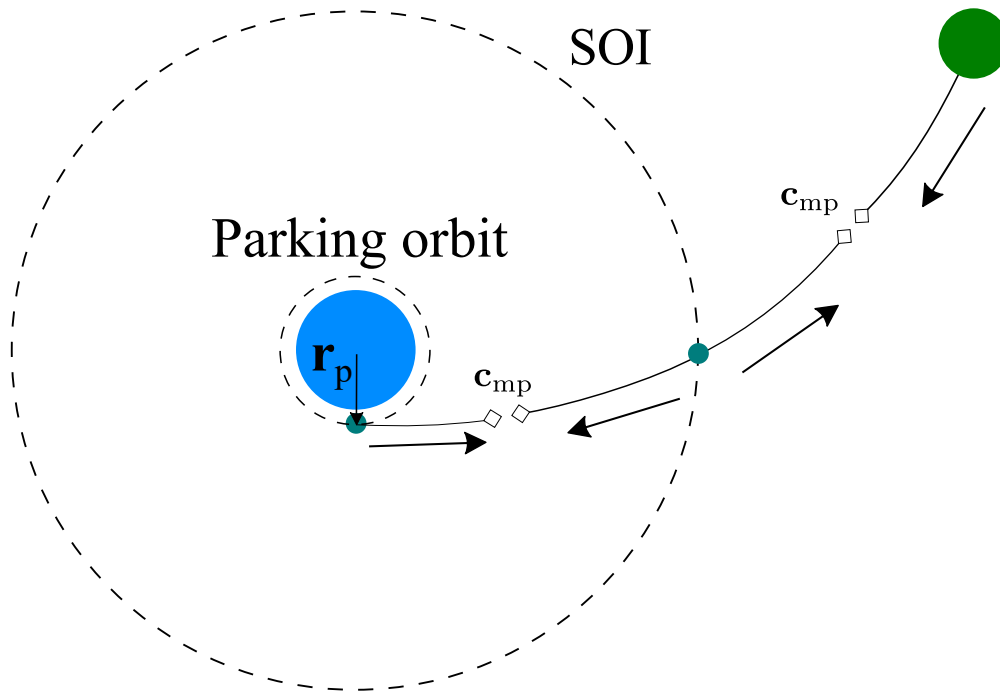American Institute of Aeronautics and Astronautics

Figure 3: High-fidelity departure from a parking orbit.

For a parking orbit departure, the magnitude of the departure maneuver (provided by the spacecraft, or the launch vehicle upper stage) is added to the list of decision variables in Table 2.

Table 3: Ephemeris-referenced parking orbit departure decision variables (in addition to Table 2).

Parameter	Description
Δv_{dep}	departure maneuver magnitude

INITIAL GUESS GENERATION

For high energy orbit regimes, formulating an initial guess for a high-fidelity flyby/launch from a ZSOI solution is fairly straightforward and robust. In this section, initial guesses/estimates for the state of the spacecraft on the SOI boundaries and at flyby periapse are indicated with asterisk (*) superscripts. The ZSOI to high-fidelity flyby model conversion process is illustrated in Figure 4.
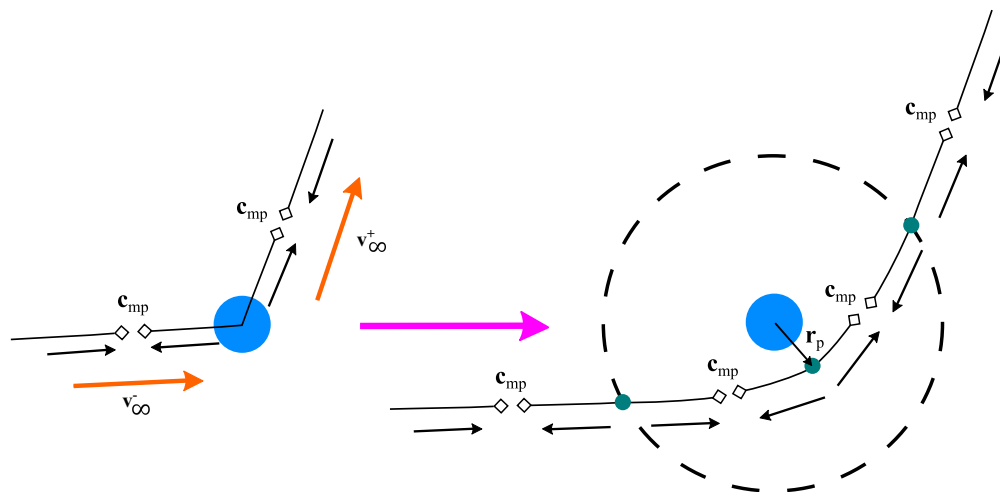

Figure 4: Conversion from a ZSOI flyby transcription to a high-fidelity flyby transcription.

First, a periapse state $[\mathbf{r}_p, \mathbf{v}_p]$ must be computed from the ZSOI flyby. The procedure outlined by Bradley and Russell[1] is outlined here in Equations (9) - (14). The periapse position unit vector is calculated as:

$$\hat{\mathbf{r}}_p = \frac{\mathbf{v}_\infty^- - \mathbf{v}_\infty^+}{\|\mathbf{v}_\infty^- - \mathbf{v}_\infty^+\|} \tag{9}$$

The periapse velocity unit vector is calculated with Equation 10:

$$\hat{\mathbf{v}}_p = \hat{\mathbf{h}} \times \hat{\mathbf{r}}_p \tag{10}$$

where

$$\hat{\mathbf{h}} = \mathbf{v}_\infty^- \times \mathbf{v}_\infty^+ \tag{11}$$

The $-/+$ superscripts refer to the incoming/outgoing flyby asymptotes. Then, an estimate for the full high-fidelity periapse state is computed as follows:

$$\begin{aligned}
\mathbf{r}_p^* &= r_p \hat{\mathbf{r}}_p \\
&= \frac{\mu_{\text{body}}}{v_\infty^{+\,2}} \left[\frac{1}{\sin(\delta/2)} - 1 \right] \hat{\mathbf{r}}_p
\end{aligned} \tag{12}$$

$$\begin{aligned}
\mathbf{v}_p^* &= v_p \hat{\mathbf{v}}_p \\
&= \left(\sqrt{\frac{2\,\mu_{\text{body}}}{r_p} + \mathbf{v}_\infty^- \cdot \mathbf{v}_\infty^+} \right) \hat{\mathbf{v}}_p
\end{aligned} \tag{13}$$

where δ is defined in Eq. (14).

$$\delta = \text{acos}\left(\frac{\mathbf{v}_\infty^- \cdot \mathbf{v}_\infty^+}{v_\infty^- \, v_\infty^+} \right), \tag{14}$$

and μ_{body} is the gravitational parameter of the target flyby body.

The periapse state estimate can now be used to compute estimates for the spherical spacecraft state vectors at the inbound/external SOI boundary and at the outbound/internal SOI boundary. In Equations (15)-() only the inbound estimates are shown, to compute outbound estimates, all variables with - superscripts must be replaced by variables with + superscripts:

1. Spherical velocity states are computed directly from the hyperbolic excess velocity vector:

$$v^* = v_\infty^- \tag{15}$$

$$vRA^* = \text{atan2}\left(v_{\infty-y}^-, v_{\infty-x}^- \right) \tag{16}$$

$$vDEC^* = \text{asin}\left(\frac{v_{\infty-z}^-}{vMAG^*} \right) \tag{17}$$

2. Convert $[\mathbf{r}_p, \mathbf{v}_p]$ to orbital elements $\{oe\}$

3. Calculate the true anomaly at the SOI interface (ν_{SOI}) using Eq. (18).

$$\nu_{\text{SOI}} = 2 \arctan\left[\sqrt{\frac{e+1}{e-1}} \tanh\left(\frac{1}{2} H_{\text{SOI}} \right) \right] \tag{18}$$

with

$$H_{\text{SOI}} \mp \text{arccosh}\left[\frac{1}{e} \left(\frac{R_{\text{SOI}}}{-a} + 1 \right) \right] \tag{19}$$

The minus/plus sign in Eq. (19) corresponds to the incoming/outgoing halves of the flyby hyperbola.

4. Convert the orbit element set (including the hyperbolic true anomaly at the SOI computed in the previous step) to a Cartesian state $[\mathbf{r}^*_{\text{SOI}}, \mathbf{v}^*_{\text{SOI}}]$. This is the Cartesian state of the spacecraft at the flyby target's SOI assuming two-body dynamics.

5. Spherical position state estimates are then computed as:

$$rRA^* = \text{atan2}\left(y^{*-}_{\text{SOI}}, x^{*-}_{\text{SOI}}\right) \tag{20}$$

$$rDEC^* = \text{asin}\left(\frac{z^{*-}_{\text{SOI}}}{r_{\text{SOI}}}\right) \tag{21}$$

A guess can also be computed for the flyby times of flight (Δt_{in}) and (Δt_{out}).

$$\Delta t_{\text{in/out}} = \frac{e \sinh(H_{\text{SOI}}) - H_{\text{SOI}}}{\sqrt{\frac{\mu_{\text{body}}}{-a^3}}} \tag{22}$$

The osculating-hyperbola-based initial-guess method outlined in this section can be used for *most* orbit regimes. For highly-perturbed orbit regimes, and especially at lower flyby encounter velocities (i.e. as the two-body approximation to the real high-fidelity trajectory degrades), this method will produce poor initial points for the optimizer.

TIME DOMAIN INTEGRATION

The example trajectories presented in the following two sections are computed using fixed-step explicit numerical integration in the time domain (eighth-order Runge-Kutta[16]). All Jacobian information is computed analytically in EMTG. Partial derivative calculations of Equation 1 rely on state transition matrix (STM) multiplication and fixed-step integration is used to ensure accurate partial derivative computations of Equations (2) and (3),[17] which dramatically improves the convergence robustness of the gradient-based NLP solver (SNOPT in this work). In order to balance numerical efficiency and propagation accuracy, the integration time step is adjusted at the trajectory match points within the flyby body SOI in Figure 2. The match point location is specified as a percentage of the half-flyby flight time.

A more natural propagation strategy would be to utilize time regularization, such a Sundman transformation,[18–20] and a corresponding modification to the variational equations. This is left as future work.

EXAMPLE: LUCY LAUNCH PERIOD GENERATION

The high-fidelity trajectory transcriptions described in this work have been applied to provide various trajectory optimization services to NASA's next Discovery mission, Lucy. Lucy will launch in 2021 and will explore the bodies known as "Trojans" that orbit the Sun at the stable L4 and L5 points ahead of and behind Jupiter. A full mission encounter itinerary (encounter and deep space maneuver (DSM) dates) is provided in Table 4. One analysis task that these optimization methods have supported is the high-fidelity rendering and optimization of Lucy's 21-day primary launch period in October/November 2021.

American Institute of Aeronautics and Astronautics

Table 4: Lucy small body target nominal encounter and DSM dates.

Event/Encounter	Event Date
Launch	October 16, 2021
DSM 1	April 19, 2022
Earth gravity assist 1	October 16, 2022
DSM 2	February 2, 2024
Earth gravity assist 2	December 13, 2024
52246 Donaldjohanson	April 20, 2025
DSM 3	April 3, 2027
3548 Eurybates	August 12, 2027
15094 Polymele	September 15, 2027
DSM 4	September 29, 2027
11351 Leucus	April 18, 2028
DSM 5	July 23, 2028
21900 Orus	November 11, 2028
Earth gravity assist 3	December 26, 2030
617 Patroclus + Menoetius	March 2, 2033

To produce the launch period trajectory set, first, a patched-conic trajectory was designed for the open of the launch period (October 16, 2021) using the EMTG software. Then, an initial guess for the high-fidelity trajectory was constructed using the method described previously in this work. This initial guess was then used to converge and optimize an end-to-end n-body trajectory in EMTG that starts from a 185 km altitude parking orbit at Earth and goes all the way to the final encounter at 617 Patroculus and models the gravity due to the Sun, all of the planetary systems in the solar system, Earth's moon, the Pluto system, cannonball SRP, and Earth's oblateness. An example Earth gravity assist 1 trajectory for launch open is shown in Figure 5.
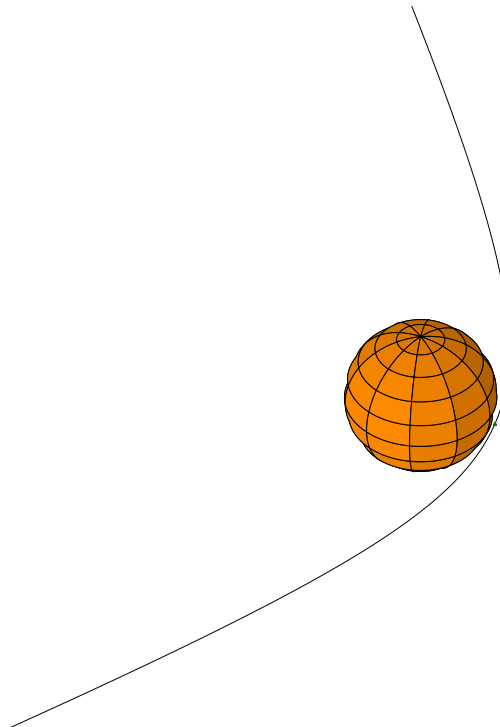

Figure 5: EGA1 for the Lucy launch open trajectory. This 300 km altitude flyby occurs on October 16, 2022.

The single launch period open high-fidelity solution was used as a seed case for all of the other 20 days in the period. The 21 individual trajectories were optimized for an hour using SNOPT and MBH. After an hour, each

trajectory was re-seeded using the best solution from the adjacent two launch dates on either side of it as an initial guess for the NLP solver (e.g., the October 30 trajectory was re-seeded with the best seed available from the October 28, 29, 30 and November 1 and 2 solutions). These re-seeded trajectories were then optimized again for an additional hour, after which the Δv and C3 solution data shown in Figure 6 obtained.
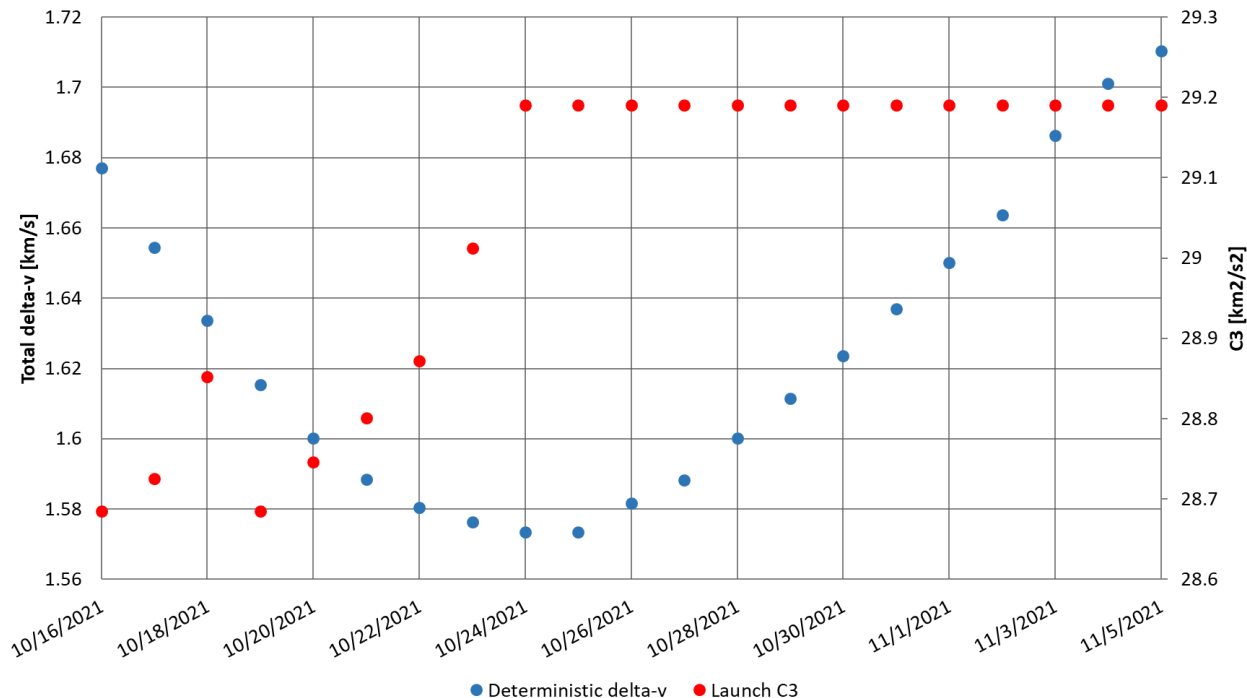

Figure 6: Deterministic mission Δv and C3 across the primary 21 day launch period.

Each of the launch date trajectories depicted in Figure 6 is an end-to-end Lucy solution computed in high fidelity and required only two hours of optimization (with seed sharing). These trajectories were all transcribed using two-point shooting, so, as a final verification step, all 21 solutions were forward targeted in General Mission Analysis Toolkit (GMAT) using a finite-burn model, as described by Englander et al.[9]

When optimizing Lucy in high fidelity, an interesting situation will arise for some days in the launch period wherein EMTG will drive the trajectory toward untargeted flybys with the moon, particularly during EGA1, resulting in a drastically reduced DSM2 magnitude. While this is an interesting display of EMTG's robust optimization capabilities, lunar flybys are not reliably available for every day in the launch period and are not practically navigable considering the short flight time between lunar orbit and periapse of the gravity assist. In order to avoid unintended lunar encounters, the spacecraft's distance from the moon is constrained to be greater than 50 000 km as it crosses the mean lunar orbit distance on the incoming and outgoing Earth gravity assist trajectories:

$$r_{\text{s/c}} - 384000 \text{ km} = 0 \tag{23}$$
$$r_{\text{moon-s/c}} - 50000 \text{ km} > 0 \tag{24}$$

These constraints are implemented by augmenting the multiple-shooting problem inside Earth's SOI to include match points interior and exterior to the mean lunar orbit sphere as shown in Figures 7 and 8.

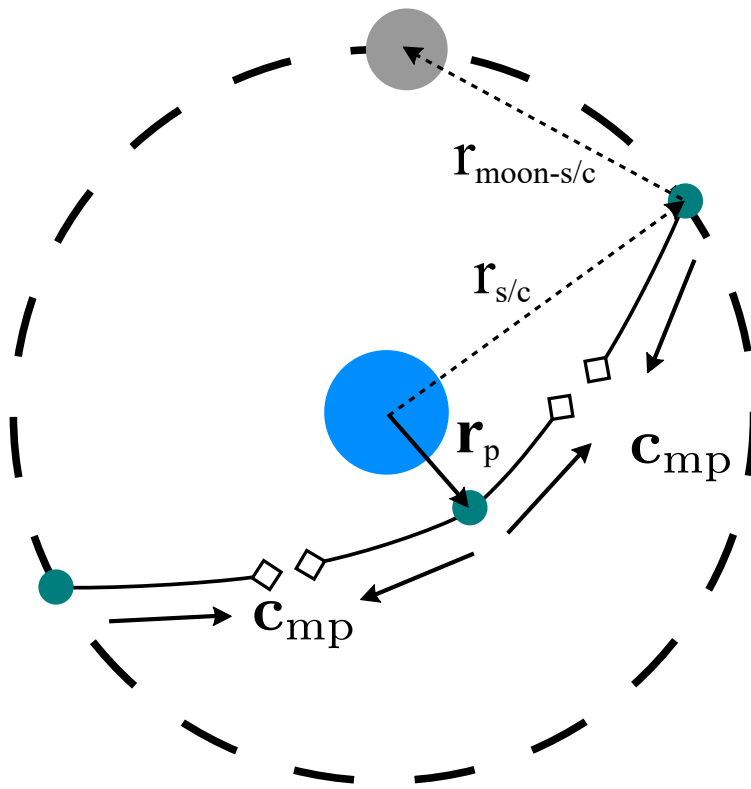American Institute of Aeronautics and Astronautics

Figure 7: Moon avoidance geometry and multiple shooting transcription. The dashed circle indicates the average lunar orbital distance.
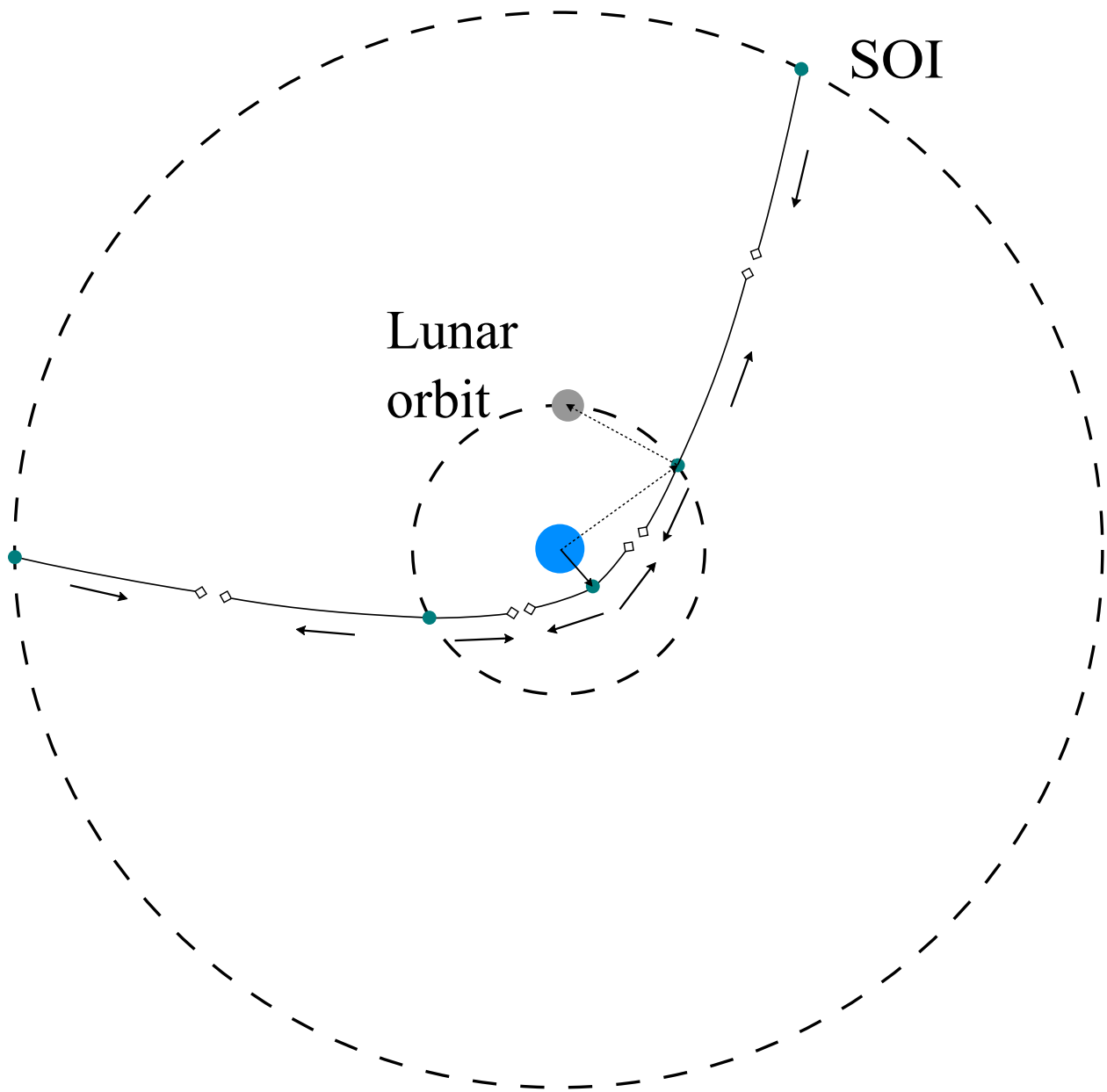
Figure 8: Augmented multiple shooting architecture inside Earth's SOI.

EXAMPLE: GAS GIANT CAPTURE

To illustrate the flexibility of the high-fidelity flyby transcription when optimizing across disparate flight regimes, an example mission to explore Europa was designed starting from a 185 km parking orbit at Earth. The mission utilizes an October 2029 Venus-Earth-Earth (VEE) trajectory option to Jupiter. The interplanetary cruise for the middle of the VEE launch period is nearly ballistic, requiring 2.35 m/s of deterministic Δv, and has a flight time of 6.195 years.

In order to reduce the required capture Δv, a satellite-aided capture is performed, which utilizes a 350 km altitude Ganymede flyby prior to the Jupiter orbit insertion (JOI) maneuver. The 929 m/s JOI maneuver places the spacecraft onto a 362.23 Jovian radii by 12.18 Jovian radii, 316 day capture orbit. The spacecraft then performs a 165 m/s perijove raise maneuver (PRM) 160 days later that sets up a flyby with Callisto with a v_∞ of 8 km/s. Four subsequent flybys of Callisto are performed that gradually decrease the spacecraft's semimajor axis and perijove distance before transitioning to a series of four 200 km altitude Europa flybys. While post-PRM tour is nearly ballistic, all maneuvers that do occur are constrained to be at least 14 days after/prior-to any flybys for navigation reasons.

The Earth-to-Jupiter cruise was first solved using a ZSOI patched-conic flyby model after which that solution was used as an initial guess for an optimization run that modeled Jupiter's gravity on the Earth-to-Jupiter phase (terminating at Jupiter's SOI) in order to obtain an accurate Jupiter arrival date. The optimizer was then set up to target a Ganymede flyby, the JOI maneuver and the first Callisto encounter using the patched-integrated ZSOI model.[b]

After converging a capture sequence, the patched-integrated ZSOI model was then used to append Galilean satellite flybys to the tour. The entire end-to-end patched-conic/patched-integrated trajectory, from Earth departure through final Europa flyby, was then used to compute a high-fidelity initial guess using the procedure described previously and converged in EMTG. The final end-to-end high-fidelity trajectory is shown in Figure 9. The Jupiter-centered tour portion of the trajectory is shown in Figure 10.
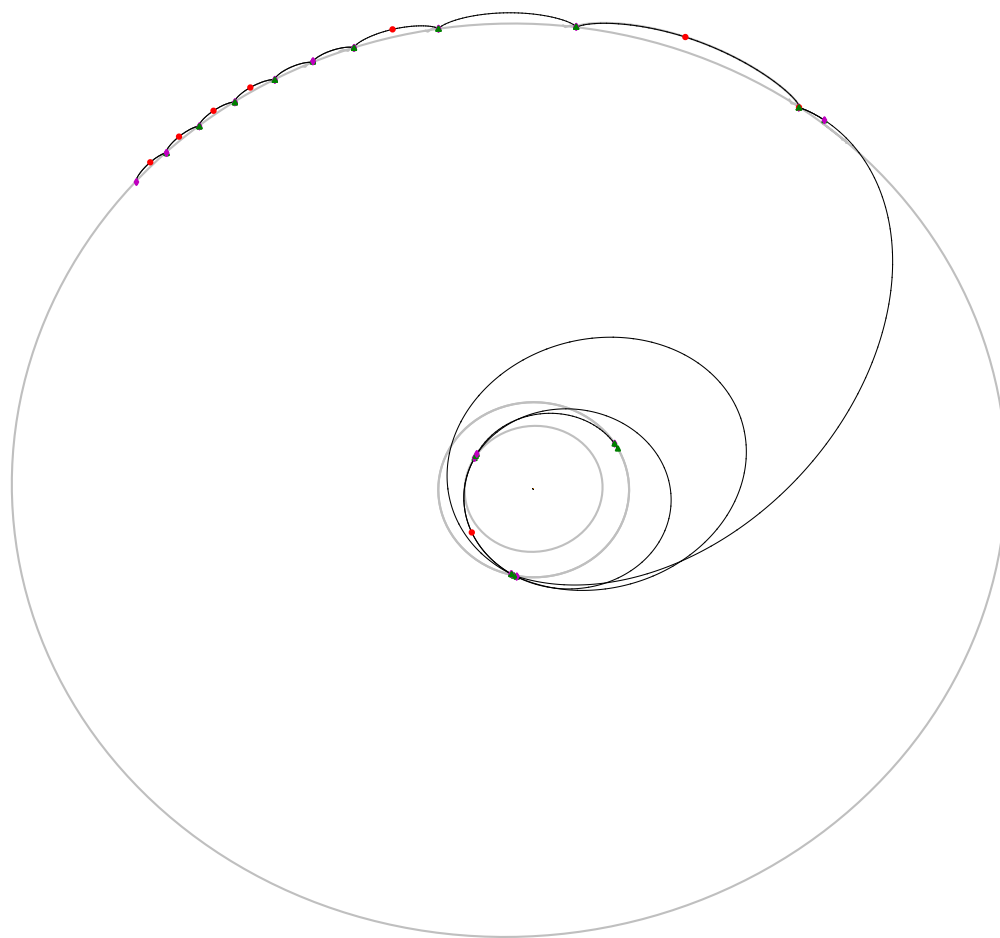

Figure 9: High-fidelity Europa Explorer trajectory starting from a 185 km altitude parking at Earth. Interplanetary flyby sequence: E-VEE-J. Tour sequence: SOI-G-JOI-CCCCC-EEEE.

[b]A two-body patched conic model is inadequate for obtaining useful Jupiter capture trajectories, even at the preliminary design stage. At the very least, the Sun's gravity must be modeled (in addition to Jupiter's) or else very optimistic capture maneuver magnitudes will be obtained.
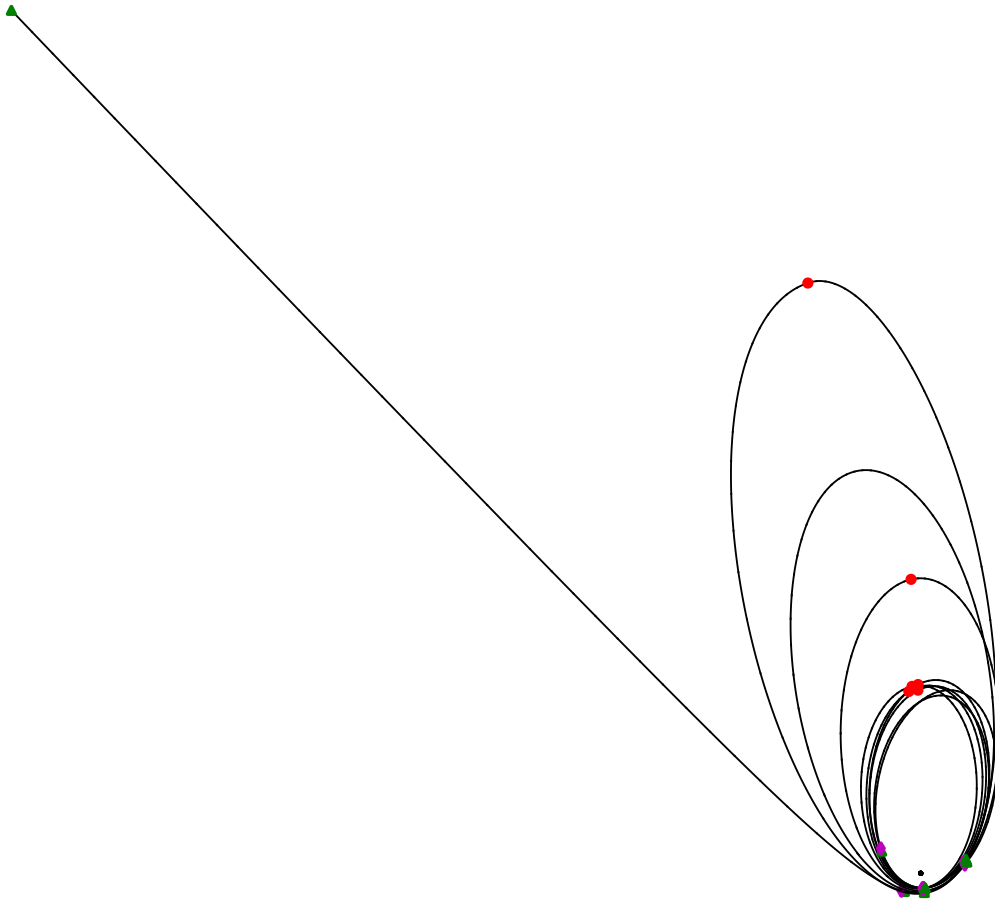
Figure 10: Moon tour from Jupiter's SOI through final Europa encounter in the Jupiter body inertial (J2000) frame. Red dots indicate maneuver locations.

In order to enable robust convergence, and to ensure that the match point constraint errors are not excessive, the various phase types in this problem (and the Lucy example in the previous section) are scaled differently. For example, the state match point constraints encoded during Earth departure/flybys, heliocentric flight, Jupiter capture, Callisto flybys, and Europa flybys are all scaled by different length unit (LU) (and the corresponding speed units computed from the LU and central body gravitational parameter μ). The different LU scale factors used for this example are provided in Table 5.

Table 5: Optimizer match point scale factors for the gas giant capture problem.

Flight Regime	LU scale factor
Launch	Earth's radius
EGAs	Earth's radius
VGA	Venus's radius
Heliocentric	1 AU
Jovian system	Mean Ganymede orbit distance
Callisto flybys	Callisto's radius
Europa flybys	Europa's radius

CONCLUSION

The difficulty associated with rendering a planetary spacecraft trajectory in a high-fidelity dynamics model warrants automating as much of the process as possible. The multiple-shooting trajectory direct transcription strategies described in this work have been demonstrated to be capable of autonomously optimizing complex mission trajectories, given a ZSOI patched-conic initial guess, and have been adopted as the primary trajectory optimization engine for

American Institute of Aeronautics and Astronautics

NASA's next Discovery-class planetary mission, Lucy. The efficacy of this trajectory optimization architecture is not limited to heliocentric regimes and can also be reliably applied to more complex dynamical regimes, such as gas giant capture scenarios (in this case a patched-integrated ZSOI initial guess was required). As with any transcription involving defect constraints, it is important to balance constraint satisfaction tolerance with convergence robustness. However, the architecture described allows for fine scaling control of the NLP constraints across multiple flight regimes. Finally, although the fixed-step time domain integration scheme used to compute the Lucy and moon tour trajectories presented in this paper is robust, in the future a regularized propagator will be implemented, which will improve the efficiency of the trajectory propagation.

ACKNOWLEDGMENTS

REFERENCES

[1] N. Bradley and R. P. Russell, "A Continuation Method for Converting Trajectories from Patched Conics to Full Gravity Models," *Journal of the Astronautical Sciences*, Vol. 61, 2014, pp. 227–254, 10.1007/s40295-014-0017-x.

[2] J. A. Atchison, M. T. Ozimek, C. J. Scott, and F. E. Siddique, "AAS 15-249 Robust High-Fidelity Gravity-Assist Trajectory Generation Using Forward/Backward Multiple Shooting," *25th AAS/AIAA Space Flight Mechanics Meeting*, Williamsburg, VA, 2015, pp. 2359–2376.

[3] J. A. Englander and B. A. Conway, "An Automated Solution of the Low-Thrust Interplanetary Trajectory Problem," *Journal of Guidance, Control, and Dynamics*, Vol. 40, No. 1, 2017, pp. 15–27, 10.2514/1.G002124.

[4] D. H. Ellison, B. A. Conway, J. A. Englander, and M. T. Ozimek, "Analytic Gradient Computation for Bounded-Impulse Trajectory Models Using Two-Sided Shooting," *Journal of Guidance, Control, and Dynamics*, Vol. 41, No. 7, 2018, pp. 1449–1462, 10.2514/1.G003077.

[5] D. H. Ellison, B. A. Conway, J. A. Englander, and M. T. Ozimek, "Application and Analysis of Bounded-Impulse Trajectory Models with Analytic Gradients," *Journal of Guidance, Control, and Dynamics*, 10.2514/1.G003078.

[6] H. F. Levison, "Lucy: Surveying the Diversity of the Trojan Asteroids: The Fossils of Planet Formation," 47th *Lunar and Planetary Science Conference*, 2017.

[7] D. Stanbridge, K. Williams, B. Williams, C. Jackman, H. Weaver, K. Berry, B. Sutter, and J. Englander, "AAS 17-632 Lucy : Navigating a Jupiter Trojan Tour," *AAS/AIAA Astrodynamics Specialist Conference*, No. August, Columbia River Gorge, Stevenson, WA, 2017.

[8] M. Vavrina, J. A. Englander, and D. H. Ellison, "Global Optimization of N-Maneuver, High-Thrust Trajectories Using Direct Multiple Shooting," *AIAA/AAS Space Flight Mechanics Meeting, AAS Paper 16-272, Napa Valley, CA*, February 14-18 2016.

[9] J. A. Englander, D. H. Ellison, K. Williams, J. McAdams, J. M. Knittel, B. Sutter, C. Welch, D. Stanbridge, and B. Kevin, "AAS 19-663 Optimization of the Lucy Interplanetary Trajectory via Two-Point Direct Shooting," *AAS/AIAA Astrodynamics Specialist Conference*, August 2019.

[10] P. E. Gill, W. Murray, and M. A. Saunders, "SNOPT: An SQP Algorithm for Large-Scale Constrained Optimization," *SIAM Rev.*, Vol. 47, No. 1, 2005, pp. 99–131, 10.1137/S0036144504446096.

[11] A. Wächter and L. T. Biegler, "On the Implementation of a Primal-Dual Interior Point Filter Line-Search Algorithm for Large-Scale Nonlinear Programming," *Mathematical Programming*, Vol. 106, June 16 2006, pp. 25–57, 10.1007/s10107-004-0559-y.

[12] J. A. Englander and A. C. Englander, "Tuning Monotonic Basin Hopping: Improving the Efficiency of Stochastic Search as Applied to Low-Thrust Trajectory Optimization," *24th International Symposium on Space Flight Dynamics, Laurel, MD*, May 2014.

[13] C. H. Yam, D. Di Lorenzo, and D. Izzo, "Constrained global optimization of low-thrust interplanetary trajectories," *2010 IEEE World Congress on Computational Intelligence, WCCI 2010 - 2010 IEEE Congress on Evolutionary Computation, CEC 2010*, 2010, 10.1109/CEC.2010.5586019.

[14] C. H. Yam, D. D. Lorenzo, and D. Izzo, "Low-thrust trajectory design as a constrained global optimization problem," *Proceedings of the Institution of Mechanical Engineers, Part G: Journal of Aerospace Engineering*, Vol. 225, February 2011, pp. 1243–1251, 10.1177/0954410011401686.

[15] "SPICE Ephemeris," August 2013. http://naif.jpl.nasa.gov/naif/.

[16] P. Prince and J. Dormand, "High order embedded Runge-Kutta formulae," *Journal of Computational and Applied Mathematics*, Vol. 7, No. 1, 1981, pp. 67 – 75, https://doi.org/10.1016/0771-050X(81)90010-3.

[17] E. Pellegrini and R. P. Russell, "On the Computation and Accuracy of Trajectory State Transition Matrices," *Journal of Guidance, Control, and Dynamics*, Vol. 39, No. 11, 2016, pp. 2485–2499, 10.2514/1.G001920.

American Institute of Aeronautics and Astronautics

[18] R. H. Battin, *An Introduction to the Mathematics and Methods of Astrodynamics, Revised Edition*. Reston, Virginia: American Institute of Aeronautics and Astronautics Inc., 1999.

[19] D. Ellison, J. Englander, and B. Conway, "A time-regularized, multiple gravity-assist low-thrust, bounded-impulse model for trajectory optimization," *Spaceflight Mechanics 2017* (J. Sims, F. Leve, J. McMahon, and Y. Guo, eds.), Advances in the Astronautical Sciences, Univelt Inc., January 2017, pp. 661–674.

[20] E. Pellegrini, R. P. Russell, and V. Vittaldev, "F and G Taylor Series Solutions to the Stark and Kepler Problems with Sundman Transformations," *Celestial Mechanics and Dynamical Astronomy*, Vol. 118, No. 4, 2014, pp. 355–378, 10.1007/s10569-014-9538-7.

American Institute of Aeronautics and Astronautics